J|A|C|S
ARTICLES
Published on Web 04/04/2006

What is Syncrystallization? States of the pH Indicator Methyl Red in Crystals of Phthalic Acid

Jason B. Benedict,[†] Dawn E. Cohen,[†] Scott Lovell,[†] Andrew L. Rohl,*[,‡,§] and Bart Kahr*[,†]

Contribution from the Department of Chemistry, University of Washington, Box 351700, Seattle, Washington 98195-1700, iVEC, "The Hub of Advanced Computing in Western Australia", Kensington, Australia, and Nanochemistry Research Institute, Curtin University of Technology, Perth, Australia

Received January 17, 2006; E-mail: kahr@chem.washington.edu

Abstract: The concept of *syncrystallization* was reinvestigated by focusing on phthalic acid (PA) grown with methyl red (MR). Crystals are alternately red and yellow in adjacent growth sectors. X-ray structures of MR and its cocrystals, revealing MR in the neutral, zwitterionic, and protonated states, as well as measurements of linear birefringence and linear dichroism of mixed crystals, were used to investigate mechanisms of PA coloring. These experiments were complemented by force field calculations of the lowest energy stable surfaces of expressed facets and energies of MR on and in crystals, as well as molecular orbital calculations of MR. Two MR species were detected in PA having distinct energies, polarizations, and face selectivities. Assignments of structures to these MRs, previously thought to be neutral and protonated, required a nuanced analysis of hydrogen bonds. The essential difference between yellow and red species is whether the MR carboxylic acid proton is inter- or intramolecularly hydrogen bound. Inferences about mixed crystal structure drawn from an examination of cocrystals of PA and MR are inconsistent with polarization spectroscopy signaling caution when using stoichiometric compounds as models of dilute solid solutions. Upon heating mixed crystals, linear dichroism diminishes and oriented, elongated pools of MR separate and pass through the bulk in directions perpendicular to the direction of elongation. These bâtonnets subsequently crystallize leaving macroscopic oriented crystals of a MR-rich phase within PA. No evidence was found for the simultaneous crystallization of MR and PA; however, the MR reorientation on heating as well as the separation and recrystallization of a MR-rich phase are distinct processes that could be embraced by the literal meaning of syncrystallization.

Introduction

In 1900, Gaubert coined the term *syncrystallization*, a contraction of synchronous crystallization, that subsequently came to describe the rare occurrence of two seemingly disparate substances that crystallize at the same time, such that oriented crystallites of one substance are overgrown by the other.[1] There are many examples of two or more things that crystallize at the same time,[2] and *syncrystallization* is sometimes used literally.[3] The meaning that evolved from Gaubert's early work is restricted in the above sense. A classic example of a supposed syncrystal studied first by Gaubert, and later by Neuhaus (see next section), is that of phthalic acid (PA) containing oriented crystallites of the acid−base indicator, methyl red (MR, CI# 13025). We could not reckon the nature of these curious objects from reading the literature alone and therefore embarked upon an experimental history in order to achieve a contemporary understanding of one *syncrystal* and the general process of syncrystallization. Syncrystallization will undoubtedly be of interest to aficionados of pathological crystallization phenomena and to those trying to orient dye nanocrystals for various technological applications.[4]

In 1996, we reported the linear dichroism (LD) of some dyed PA crystals but gave no mention of MR.[5] Subsequently, we reported that adjacent PA growth sectors were colored yellow and red by MR, respectively.[6] In reviews, we published a photograph of one such crystal[7] and paintings of them by

[†] University of Washington.
[‡] iVEC.
[§] Curtin University of Technology.

(1) Gaubert, P. *Bull. Soc. Fr. Min.* **1900**, *23*, 211−221.
(2) Bernstein, J.; Davey, R.; Henck, J.-O. *Angew. Chem., Int. Ed.* **1999**, *38*, 3440−3461.
(3) (a) Pertsev, A. N. *Geochem. Int.* **2004**, *42*, 1078−1085. (b) Mascherpa-Corral, D.; Mascherpa, G.; Chauvet, A. *J. Solid State Chem.* **1993**, *103*, 298−306. (c) Riera, A. M. I.; Pourroy, G.; Poix, P. *J. Solid State Chem.* **1992**, *101*, 195−198. (d) Chanh, N. B.; Clastre, J.; Gaultier, J.; Haget, Y.; Meresse, A.; Lajzerowicz, J.; Filhol, A.; Thomas, M. *J. Appl. Crystallogr.* **1988**, *21*, 10−14. (e) Brianso, M. C. *Acta Crystallogr., Sect. B* **1981**, *37*, 618−620. (f) Thayer, J. P. *Am. J. Sci.* **1980**, *280*, 269−283. (g) Petit, B.; Bourlang, C. *Comptes Rendus Hebd. Seances Acad. Sci. Ser. C* **1973**, *C276*, 1485−1488.
(4) Kaneko, Y.; Onodera, T.; Kasai, H.; Okada, S.; Oikawa, H.; Nakanishi, H.; Fukuda, T.; Matsuda, H. *J. Mater. Chem.* **2005**, *15*, 253−255.
(5) Mitchell, C. A.; Lovell, S.; Thomas, K.; Savickas, P.; Kahr, B. *Angew. Chem., Int. Ed. Engl.* **1996**, *35*, 1021−1023.
(6) Kurimoto, M.; Bastin, L. D.; Fredrickson, D.; Gustafson, P. N.; Jang, S.-H.; Kaminsky, W.; Lovell, S.; Mitchell, C. A.; Chmielewski, J.; Kahr, B. In *Morphology and dynamics of crystal surfaces in complex molecular systems*; De Yoreo, J. J., Casey, W. H., Malkin, A. J., Vlieg, E., Ward, M. D., Eds.; Materials Research Society: Pittsburgh, PA, 2001; Vol. 620, pp M981−M9810.
(7) Kahr, B.; Gurney, R. W. *Chem. Rev.* **2001**, *101*, 893−951.

10.1021/ja0601181 CCC: $33.50

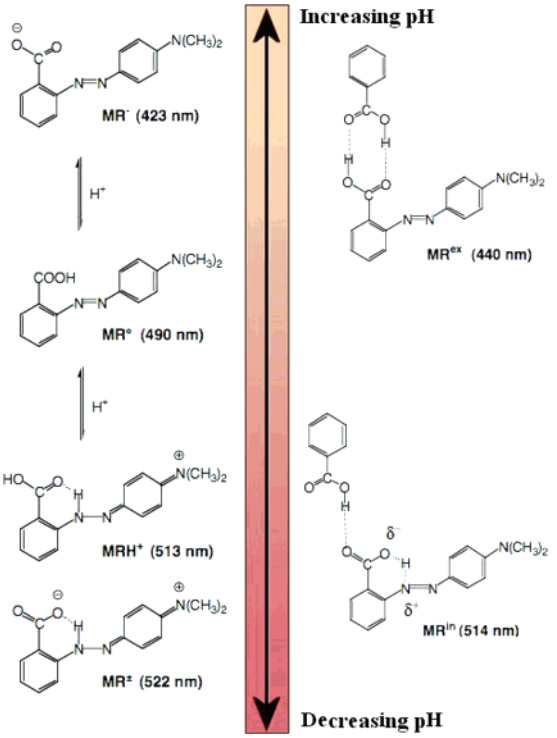

Figure 1. Left column: methyl reds identified in solution equilibria. Right column: proposed high and low energy absorbing H-bonding patterns with aromatic acids. Center bar: range of colors observed in mixed crystals of phthalic acid with methyl red. The data 423 (aq.), 513 (aq.), and 522 nm (aq.) are from ref 26. The data 490 (EtOH), 440 (PA), and 514 (PA) nm are from this work.

Vasquez.[8] As MR is a classic acid−base indicator, it was natural to assume that the red color was associated with the protonated MRH^+ and the orange−yellow was from neutral MR° (Figure 1). However, nothing about our PA/MR crystals resembled descriptions from the last century of crystallites of MR oriented within PA. Where was the so-called syncrystal, and what was it?

Syncrystallization

Lehmann first discovered that PA crystals, grown from dye solutions, are often colored in particular growth sectors.[9] He did not use MR, although he did report pleochroic crystals when PA was grown in the presence of related azo dyes, chrysoidin (CI# 11270) and methyl orange (CI# 13020). The crystallization of PA from dye solutions was further studied by Gaubert.[10] Initially, he introduced the term syncrystallization to describe isomorphous barium, lead, and strontium nitrates grown in the presence of methylene blue (CI# 52015).[1] He concluded that microcrystals of the dye were oriented within heavily colored lead nitrate crystals because deposition usually only occurred when the dye and salt were saturated in solution. When Gaubert first studied dyed PA crystals, though not with MR, he was emphatic that these were not nitrate-like syncrystals[10] because PA was colored even when the dye was under-saturated in the growth solution. Nevertheless, Gaubert left open the possibility of using the term syncrystallization for coloring transparent crystals with dilute dye solution.[11] A generation later, he reversed himself by restricting syncrystallization to those cases of colored crystals that could only be produced at great dye strength,[12] prompting Buckley to characterize Gaubert's work as "intermittent and discursive".[13] Bunn argued that Gaubert's conclusion of crystals within crystals was given "without much evidence."[14]

In 1937, Gaubert returned to PA with MR.[15] He reported that these highly dichroic dyed crystals became more or less isotropic in their absorption for light incident along [010] when heated to temperatures of approximately 150 °C. Gaubert assumed that dye molecules diffused through the PA lattice. Upon cooling these crystals, he observed the formation of oriented crystalline *bâtonnets*[16] within the bulk PA lattice and concluded that microcrystals of the dye were oriented within the host.

Gaubert's concept of syncrystallization predated X-ray diffraction. It gave way to epitaxy, the oriented overgrowth of one crystalline substance on another. Neuhaus, a pioneering epitaxy researcher,[17] brought his experience to studies of dye inclusion crystals and thereby carried some of Gaubert's results into the post-diffraction era. By measuring lattice constants of crystalline dyes and the salts with which they had ostensibly syncrystallized, Neuhaus proposed epitaxial relationships. In hindsight, it appears to us that Neuhaus tried to force lattice matches upon host/guest pairs.[18] For example, in support of epitaxial growth, he indicated that four-thirds of the (110) *d*-spacing in PA was approximately equal to the (110) spacing in MR, and that three halves the $[\bar{1}10]$ vector in PA was equal to the $[\bar{1}10]$ vector in MR. While this kind of lattice matching may well make sense in some cases, it is little more than numerology in others.

Results

Phthalic Acid. Phthalic acid (PA) crystals have an unusually rich habit. The following forms have been observed: {010}, {001}, {110}, {111}, {021}, {112}, $\{12\bar{1}\}$, {131}, $\{11\bar{1}\}$.[19] Their relative importance is sensitive to solvent and additives. The {010} face is dominant when PA is crystallized from water but absent when crystallized from ethanol. Figure 2 illustrates the idealized habit of PA when grown from an evaporating 20% $EtOH/H_2O$ solution at room temperature.

The crystal structure of PA (space group *C*2/*c*, Table 1) was optimized with the GULP simulation engine[20] using the CVFF force field.[21] The Coulombic interactions, evaluated using the Ewald sum, and the long-range van der Waals terms described by a Lennard-Jones potential were truncated at 12 Å. This yielded a cell that was 2.1% smaller than the experimental cell

(8) Kahr, B.; Vasquez, L. *CrystEngComm* **2002**, 514−516.
(9) Lehmann, O. *Z. Phys. Chem.* **1891**, *8*, 543−553; *Ann. Phys. Chem.* **1894**, *51*, 47−76.
(10) Gaubert, P. *Bull. Soc. Fr. Min.* **1905**, *28*, 286−304; *Comptes Rendus Acad. Sci. Paris* **1906**, *142*, 219−221.
(11) Gaubert, P. *Soc. Chim. Phys.* **1911**, *1*, 33.
(12) Gaubert, P. *Comptes Rendus Acad. Sci. Paris* **1935**, *200*, 1120−1122.
(13) Buckley, H. E. *Crystal Growth*; Wiley: New York, 1951; p 346.
(14) Bunn, C. W. *Proc. R. Soc. London, Ser. A* **1933**, *141*, 567−593.
(15) Gaubert, P. *Comptes Rendus Acad. Sci. Paris* **1937**, *204*, 599−601.
(16) The choice of *bâtonnet* to describe the separated dye particles was likely influenced by the introduction of this term into the liquid crystal literature at about the same time. See: Friedel, G. *Ann. Phys.* **1922**, *18*, 273−474.
(17) Gebhardt, M., Neuhaus, A., Hellwege, K.-H., Hellwege, A. M., Eds. *Epitaxy Data of Inorganic and Organic Crystals Landolt-Börnstein: Numerical Data and Functional Relationships in Science and Technology*; New Series Group 3, Condensed Matter; Springer: Berlin, 1972; Vol. 8.
(18) Neuhaus, A. *Z. Krist.* **1941**, *103*, 297−327. To compare Neuhaus's triclinic methyl red cell ($a = 8.45$ Å, $b = 11.6$ Å, $c = 9.30$ Å, $\alpha = 115°$, $\beta = 125°$, $\gamma = 66°$) with our own, we must adopt the following cell based on vectors derived from the monoclinic crystal in Table 1: [010] = 8.50 Å, [111] = 11.72 Å, $[\bar{1}10] = 9.16$ Å, $\alpha = 116.5°$, $\beta = 124.6°$, $\gamma = 66.3°$.
(19) Lindenberg, W. *N. Jahr. Min. Ab.* **1956**, *89*, 149−181.
(20) Gale J. D.; Rohl A. L. *Mol. Simul.* **2003**, *29*, 291−341.
(21) Dauber-Osguthorpe, P.; Roberts, V. A.; Osguthorpe, D. J.; Wolff, J.; Genest, M.; Hagler, A. T. *Proteins: Struct., Funct., Genet.* **1988**, *4*, 31−47.

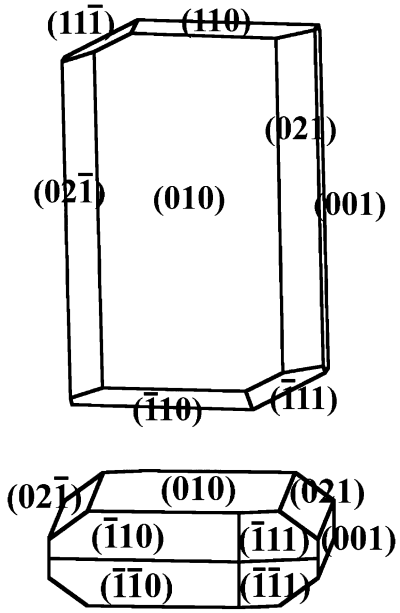

Figure 2. Idealized habit of phthalic acid grown from 20% ethanol/water solution.

listed in Table 1.[22] The structures of all possible terminations of the 15 surfaces with the largest d_{hkl} were then generated using the GDIS program[23] and optimized in GULP.[20]

The surface and attachment energies, the energies of surfaces compared to the bulk per unit surface area, and the energies released when a new slice of depth d_{hkl} is attached to a crystal face, respectively, were calculated for the 9 (*hkl*) faces with the largest inter-planar spacings. They are listed in Table 2. The most striking feature is that the values for the surface energies as well as for the attachment energies span small ranges. This is reflected in the calculated growth morphology (based on attachment energies) and equilibrium morphology (based on surface energies), where five and nine forms are present, respectively. Such a preponderance of forms is rare but is consistent with the sensitivity of the morphology to growth conditions.[19]

Methyl Red. Methyl red (MR) has complex acid−base equilibria.[25] Four different forms have been proposed in various solutions: neutral (MR°), zwitterionic ($MR^{\pm}$), protonated (MRH^{+}), and deprotonated (MR^{-})[26] (Figure 1) supposedly corresponding to absorption maxima at 490 (EtOH), 522 (aq.), 513 (aq.), and 423 (aq.) nm, respectively. When used as a pH indicator, the red color of MR is generally ascribed to MRH^{+}, although a comparable absorption at 522 nm has been assigned to the red $MR^{\pm}$ in mildly acidic ($3 < pH < 6$) solutions. Despite the barely distinguishable red colors of $MR^{\pm}$ and MRH^{+}, the isosbestic point observed by titration indicates the presence of two species at low pH. The pK_a of MRH^{+} is 2.1 ± 0.1 in water.[26] The predominant species in the solution from which we grow mixed crystals was the zwitterion, $MR^{\pm}$ ($\lambda_{max} = 522$ nm).

To further verify that the species in *slightly* acidic, aqueous solutions is not MRH^{+}, we analyzed the ^{1}H NMR spectrum of MR in three CD_3OD solutions: (1) 5.9×10^{-3} M MR; (2) the same, saturated with PA (0.12 M, $pK_{a1} = 2.95$);[27] (3) the same as (1) with HCl (0.12 M). In (2), the resulting spectrum was essentially the superposition of the ^{1}H NMR spectra of PA and MR. In (3), the addition of HCl produces a sharp downfield shift of the aromatic region, consistent with protonation.[28]

We obtained a high-resolution crystal structure of MR. The published structure[29] was based only on the refinement of the heavy atom positions ($R = 0.093$); protons were ill-defined. After locating and anisotropically refining heavy atoms, a difference map revealed the positions of all hydrogens, the placement of which are pivotal in understanding PA/MR mixed crystals. (Throughout, the symbol PA/MR indicates nonstoichiometric mixed crystals, whereas PA·MR indicates a *cocrystal*. Cocrystal implies a stoichiometric relationship between more than one component, whereas a *mixed crystal* is nonstoichiometric.) The MR° carboxylic acid proton was located on the oxygen nearest an azo nitrogen and intramolecularly hydrogen bonded to it (N−O = 2.591(2) Å). The molecules pack as head-to-tail dimers. MR has a distinctly quinoidal geometry in the crystalline state; the aromatic bond length variation in the dimethylaminophenyl group is 0.050 Å. Summaries of crystallographic data are given in Table 1.

To probe the relative stabilities of the neutral species compared to the zwitterion, we undertook first principles calculations. The work of Tuble and co-workers on norleucine demonstrates that its zwitterion is unstable in vacuo and requires the presence of a solvent for stabilization.[30] To see if the same is true for the larger MR molecule, potential energy was computed as a function of the N to H distance between 0.95 and 2.0 Å in 0.05 Å increments. The Gaussian 03 program was employed.[31] The 6-31G* basis set was used with the Hartree−Fock, B3LYP, and MP2 methodologies. The calculations were performed both in vacuo and under aqueous conditions using the continuum IEFPCM solvation model. The results of these calculations are summarized in Figure 3.

All three methodologies predict that the zwitterion is not stable in vacuo, although all three curves show a change in slope at about 1.05 Å. Adding solvation via the continuum IEFPCM model results in a double well potential in each case. The zwitterion minimum is shallow, particularly in the MP2 curve. The B3LYP curves are very similar to the MP2 curves; these are quite different than the HF curves. All subsequent first principles calculations have used the B3LYP hybrid functional with the larger 6-311G** basis set as they are much quicker than the MP2 calculations but offer similar accuracy. MR° is calculated to be 37 kJ/mol lower in energy than $MR^{\pm}$, with N−H distances of 1.75 and 1.05 Å, respectively.

(22) CVFF relaxed PA unit cell: $a = 4.837$ Å, $b = 14.382$ Å, $c = 9.877$ Å, $\beta = 95.701°$.
(23) Fleming, S. D.; Rohl, A. L. *Z. Kristallogr.* **2005**, *220*, 580−584.
(24) (a) Ermer, O. *Helv. Chim. Acta* **1981**, *64*, 1902−1909. (b) Veenendaal, A. L.; MacGillavry, C. H. *Acta Crystallogr.* **1954**, *7*, 775. (c) van Schalkwyk, T. G. D. *Acta Crystallogr.* **1954**, *7*, 775.
(25) Ramette, R. W.; Edward, A. D.; Kelly, P. W. *J. Phys. Chem.* **1962**, *66*, 527−532.
(26) Drummond, C. J.; Grieser, F.; Healy, T. W. *J. Chem. Soc., Faraday Trans. I* **1989**, *85*, 561−578.
(27) Singh, A. K.; Ghosh, J. C. *J. Indian Chem. Soc.* **1983**, *60*, 702−704; **1985**, *62*, 158−160.
(28) A comparison of the six most downfield peaks in the spectra was the following for MR (MR in 0.12 M PA) [MR in 0.12 M HCl]: $\delta = 7.974$ ppm (7.983) [8.069]; 7.948 (7.959) [8.040]; 7.786 (7.788) [7.997]; 7.760 (7.762) [7.969]; 7.686 (7.667) [7.787]; 7.655 (7.635) [7.755].
(29) Moreiras, D.; Solans, J.; Solans, X.; Marivitlles, C.; Germain, G.; Declerq, J. P. *Cryst. Struct. Comm.* **1980**, *9*, 921−924.
(30) Tuble, S. C.; Anwar, J.; Gale, J. D. *J. Am. Chem. Soc.* **2004**, *126*, 396−405.
(31) Frisch, M. J.; et al. *Gaussian 03*, revision C.02; Gaussian, Inc.: Wallingford, CT, 2004.

Table 1. Crystallographic Data

substance	MR	0.5 PA·MR	2,5-DHB·MR	MR·HBr·H_2O	PA[24]
formula	$C_{15}H_{15}N_3O_2$	$C_{19}H_{18}N_3O_4$	$C_{22}H_{21}N_3O_6$	$C_{15}H_{18}BrN_3O_3$	$C_8H_6O_4$
mol. wt (amu)	269.30	352.36	423.42	368.23	166.13
space group	$P\bar{1}$	$C2/c$	$P2_1/c$	$P2_1/c$	$C2/c$
a (Å)	8.2370(5)	9.0830(5)	7.0220(3)	7.8900(2)	5.0698(4)
b (Å)	8.4990(6)	14.1850(7)	13.5530(7)	11.8980(4)	14.318(1)
c (Å)	11.211(1)	26.653(2)	21.840(1)	16.6620(7)	9.6305(5)
α (deg)	92.478(3)	90	90	90	90
β (deg)	110.281(3)	98.042(4)	99.984(2)	92.568(1)	93.260(4)
γ (deg)	113.705(3)	90	90	90	90
V_{cell} (Å^3)	658.66(9)	3400.3(4)	2047.0(2)	1562.58(9)	697.81(4)
T (K)	130 (2)	130 (2)	298	130 (2)	298
Z	2	8	4	4	4
R_1	0.0635	0.0757	0.0625	0.0375	0.040
wR_2	0.1615	0.2338	0.1530	0.0977	not reported
GOF	0.990	1.012	0.925	0.999	not reported
e_{min}/e_{max} (e/Å^3)	0.216/−0.269	0.373/−0.393	0.288/−0.221	0.504/−0.777	0.44/−0.22

Table 2. Computed Phthalic Acid Surface and Attachment Energies for Various Facets for the Relaxed Unit Cell

face	d_{hkl} (Å)	surface energy (J m^{-2})	attachment energy (eV/mol)
(020)	7.172	0.324	−1.055
(021)	5.783	0.267	−1.032
(002)	4.889	0.258	−1.157
(110)	4.594	0.249	−1.141
(111)	4.310	0.329	−1.328
(02$\bar{2}$)	4.039	0.291	−1.316
(11$\bar{1}$)	4.021	0.204	−1.031
(11$\bar{2}$)	3.509	0.355	−1.775
(130)	3.405	0.308	−1.653
(04$\bar{1}$)	3.367	0.305	−1.350
(13$\bar{1}$)	3.284	0.313	−1.557
(112)	3.207	0.228	−1.461
(131)	3.151	0.293	−1.800
(02$\bar{3}$)	2.967	0.293	−1.328
(13$\bar{2}$)	2.885	0.340	−1.701

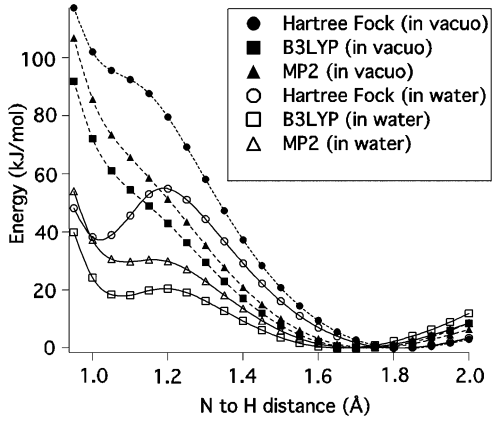

Figure 3. Computed energies of the MR molecule as a function of the N to H distance using various first principles methods. The dashed lines are in vacuo calculations, and the solid lines are the results in water using the continuum IEFPCM model (see text).

MR° in the crystal structure was also slightly quinoidal; the aromatic bond length variation in the dimethylamino group was 0.46 Å. The calculated gas phase antiparallel dimer was only slightly more quinoidal (aromatic bond length variation = 0.53 Å). In other words, the centrosymmetric arrangement of MR°s induces only a modest distortion of the individuals.

Cocrystals. Attempts to grow PA/MR mixed crystals at high dye concentrations, at or above 3×10^{-4} M MR, precipitated 0.5:1 cocrystals of PA and MR (0.5 PA·MR).[32] Crystallographic parameters are given in Table 1. Again, electron density difference maps revealed all protons. The MR molecule in the cocrystal structure was not protonated MRH^+, nor the NH^+ zwitterionic tautomer $MR^{\pm}$. Nevertheless, MR in the 0.5 PA·MR cocrystal was slightly quinoidal (Figure 4), with an aromatic bond length variation in the dimethylaminophenyl ring of 0.057 Å, matching surprising well the geometry of the calculated MR° monomers or dimers. Similarly, the cocrystals had an intramolecular H-bond to the nearest azo nitrogen atom (N−O = 2.549(4) Å). There is a single H-bond to a neighboring PA donor that sits on a special position, the diad axis, giving rise then to the 1:2 stoichiometry. Pairs of MRs in 0.5 PA·MR are antiparallel and virtually superimposable on the dimers in the pure MR crystal structure.

Given that O-protonated MR° was observed in both the MR and 0.5 PA·MR, we aspired to establish structures of the purported red species MRH^+ and $MR^{\pm}$ as models of the species possibly contained within PA mixed crystals (see next section). MR·HBr·H_2O crystals were prepared from aqueous solutions to which HBr had been added dropwise. A proton was unambiguously located on an azo nitrogen atom nearest the COOH group. The ion is quinoidal. The aromatic bond length variation in the dimethylaminophenyl group is 0.104 Å with π electrons considerably more localized than in MR°.

Whither the zwitterion, $MR^{\pm}$? We ultimately observed it while analyzing cocrystals of methyl red with another aromatic acid, 2,5-dihydroxybenzoic acid (2,5-DHB), deposited from ethanol solutions. Figure 5 shows the hydrogen bonding contacts that MR makes with two 2,5-DHB molecules. Because two acid molecules serve as H-bond donors to the MR carboxylic acid group, the latter's proton is passed to the azo nitrogen atom. The quinoidal character of $MR^{\pm}$, as judged from the dimethylaminobenzene aromatic bond length variation (0.69 Å), was intermediate between that of MR° and MRH^+. However, molecules are pairwise antiparallel in precisely the manner as observed for MR° in MR and 0.5 PA·MR crystal structures.[33]

Mixed Crystals. Mixed crystals of PA and MR (PA/MR) were easily grown on microscope slides (Figure 6).[34] We observed {010} plates with {021}, {110}, and {001} facets. The crystals deposited were stunning in their dual color. They contained a red hourglass pattern associated with the {001} growth sectors as well as a yellow−orange tinge throughout as

(32) Thin red plates were collected. The crystals first deposited, and those from the recrystallization had the same unit cell.

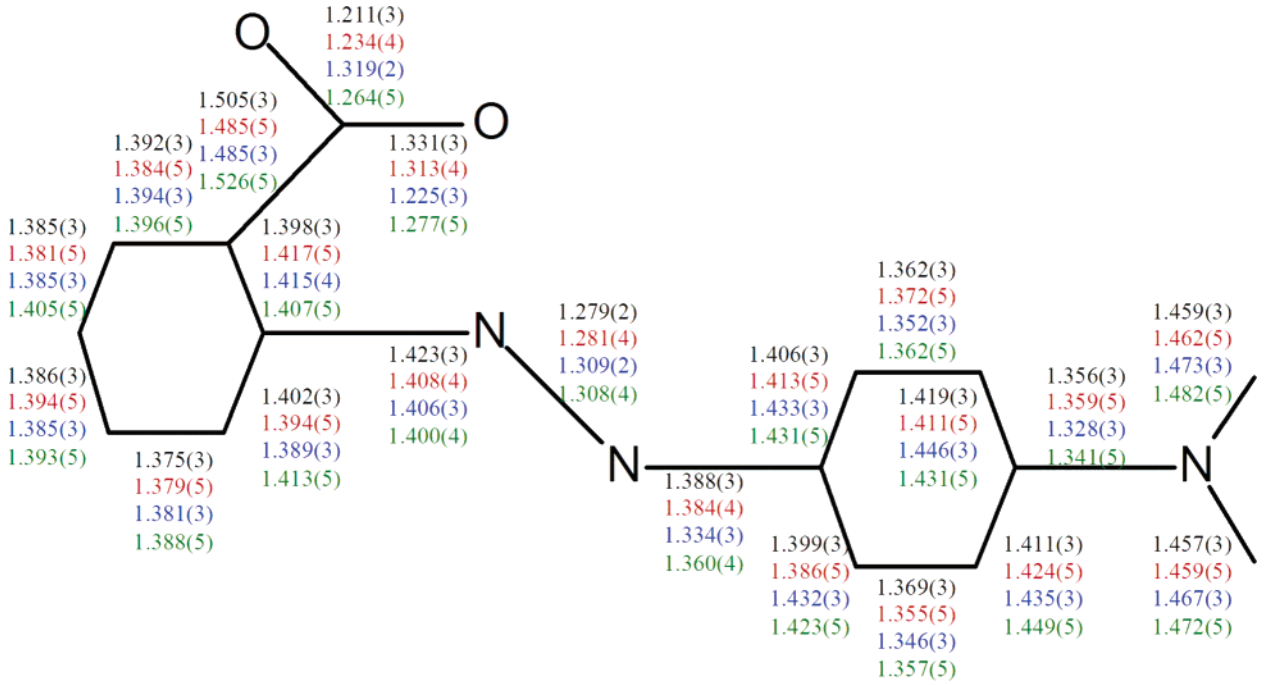

Figure 4. MR skeleton with crystallographic bond lengths of pure MR crystal (black), 0.5 PA·MR (red), MR·HBr·H_2O (blue), and 2,5-DHB·MR (green).

a result of dye adsorption by the {010} and {110} faces. Larger crystals (~2 mm^3) were obtained by slow evaporation. The dye content, determined by measuring the absorbance of dissolved mixed crystals, was typically 3.3×10^{-3} wt % when precipitated from solutions containing 1.8×10^{-3} wt % ($\epsilon_{MR(EtOH,490nm)} = 3.08 \times 10^3\ M^{-1}\ cm^{-1}$). PA crystals concentrate MR and clean solutions of it. The segregation coefficient is 1.8.

Crystals were grown on slides over a range of MR concentrations (5×10^{-4} to 1×10^{-5} M MR), albeit a small range in which dye could be detected and mixed crystal growth proceeded. There was no evidence of a concentration dependence of the two species in the spectra. Aggregation therefore does not seem to play a large part in mixed crystal phenomenology.

The crystals are strongly dichroic for polarized light incident upon (010) with maximum absorbances for both the yellow and red species when the input polarization was aligned at 42° to the crystallographic *a* axis. The vibration directions are very nearly the [201] and [20$\bar{1}$] directions.[35] Larger crystals grown by slow evaporation were cleaved along (101) in slices approximately 0.5 mm thick, allowing dichroic ratios to be measured for light polarized along [010] and [10$\bar{1}$] (Figure 7). The polarized absorption spectra of the various growth sectors are illustrated in Figure 8.

The observed visible absorption bands of MR originate from $\pi-\pi^*$ electronic transitions. MR exists within PA crystals in

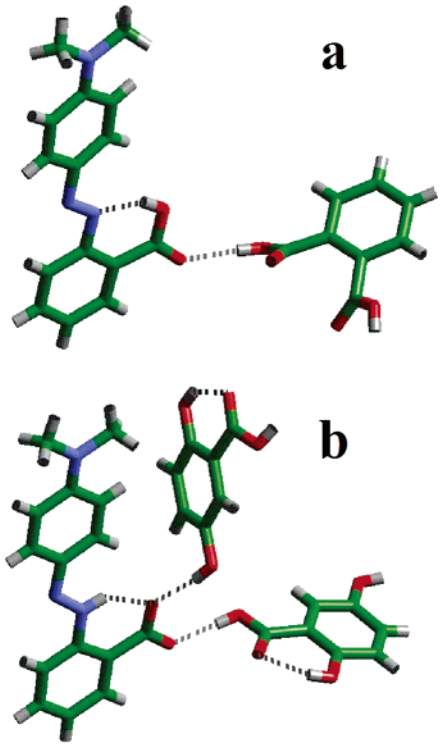

Figure 5. Hydrogen bonds of MR with (a) PA and with (b) 2,5-DHB, in respective cocrystals.

(33) Absorption spectra of MR in various crystalline environments were obtained by smearing single crystals between glass slides in order to produce fragments thin enough to transmit light. The λ_{max} for crystalline MR, 0.5 PA·MR, 2,5-DHB, $MR^{\pm}$, and MR·HBr·H_2O were 510, 509, 476, and 518 nm (with a pronounced shoulder at 610 nm), respectively. These data are curious in that the spectra of MR and 0.5 PA·MR are identical, despite the H-bonding in the latter case of MR to PA, and are unusually red. The latter shift could be a consequence of charge-transfer interactions. Also of note is the comparative blue shift of 2,5-DHB·MR. This could be a consequence of a hypsochromic shift due to close antiparallel dipoles. On the other hand, we acknowledge that these spectra were made under nonideal conditions (crushed crystals) with directions unspecified. Collective interactions as yet undetermined could dominate the spectra of single dye crystals. See: Anex, B. G. *Mol. Cryst.* **1966**, *1*, 1−36.

(34) Larger crystals can be obtained by slow evaporation of a 20% EtOH/H_2O solution (0.75 g PA/mL) at room temperature; however, care must be taken to retrieve the crystals approximately 6−8 h after nucleation to ensure crystals are grown with a nearly constant solvent composition. Typical MR concentration was 5×10^{-5} M. Absorbance measurements of dissolved mixed crystals grown from 1.8×10^{-3} mass % starting solution were found to contain 3.3×10^{-3} mass %.

(35) These directions, with an angle of 87° between them, are not strictly the vibration directions, but they provide a convenient reference. As (010) is highly birefringent ($n_{[20\bar{1}]} = 1.696$, $n_{[201]} = 1.456$), a Lorentz approximation, $A_{obs} = [(n^2 + 2)^2/9n] \times A_{corr}$, was applied where *n* and *A* are the refractive index and absorbance in similar directions, respectively.

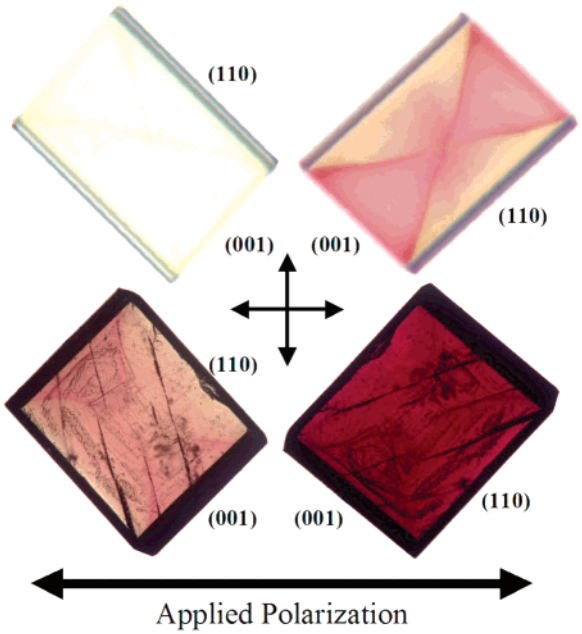

Figure 6. Pair of phthalic acid crystals grown in the presence of methyl red, each in two positions with respect to applied plane polarized light. Crystals grown from solutions containing 5×10^{-5} M MR. Top: Crystal grown on a glass slide (0.8 mm × 0.45 mm). Bottom: Crystal grown in crystallizing dish by slow evaporation (5 mm × 7 mm). Crossed arrows represent crystallographic vibration directions.

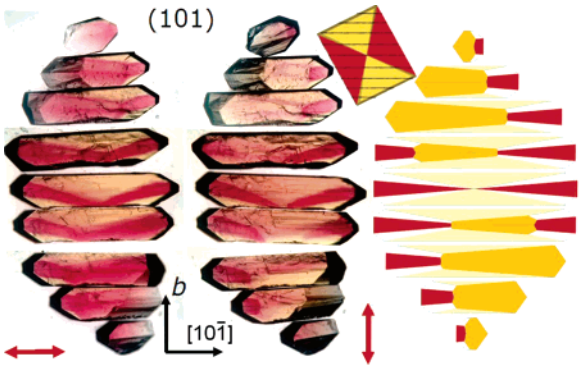

Figure 7. Contrast enhanced photographs of (101) slices of a MR dyed PA crystal viewed normal to the cleavage plane. Applied polarization indicated with red arrows. Right column illustrates idealized (101) slices of {010} plate laid side by side. Inset shows {010} sliced to give rightmost composite illustration made with WinXMorph (Kaminsky, W. *J. Appl. Crystallogr*. **2005**, *38*, 566−567).

at least two states, on the basis of energy, one absorbing in the green (513 nm) part of the visible spectrum that appears red, and the other in the blue (440 nm) part of the spectrum, appearing yellow (Figure 8).[36] The absorption of the yellow species is closest in energy to MR^-. However, existence of MR^- in the acid crystals is unlikely. The hypsochromic shift is more likely the consequence of the MR carboxylic acid proton participating in a strong "external" intermolecular H-bond with a phthalic acid acceptor, MR bound as an $R_2^2(8)$ dimer (MR^{ex}, Figure 1).[37]

In their electronic structures, MR^{ex} and MR^- should resemble one another. To test this notion, we carried out ZINDO calculations of the electronic transitions of the various MR species conjectured. To model the MR^{ex} species, a MR H-bound to benzoic acid forming an $R_2^2(8)$ dimer was constructed.[38] The energies of the transitions with the greatest oscillator strengths for MR^-, MR^{ex}, MR°, $MR^{\pm}$, and MRH^+ were 309, 359, 386, 491, and 467 nm, respectively.[39] The transition for MR^{ex} is intermediate in energy when compared to MR^- and MR°, precisely what is observed experimentally. The virtually parallel electric dipole transition moments were used as the molecular axes for all orientation measurements.

On the basis of studies of the protonation of MR in solution and in cocrystals, we have concluded that the red species is unlikely to be MRH^+ as we had earlier conjectured.[7] The absorbance of the red species is intermediate with respect to MR° and $MR^{\pm}$, presumably a consequence of the "internal" location of the COOH proton residing between the oxygen and nearest azo nitrogen. We hereafter call this species MR^{in}.

The yellow species (MR^{ex}, 440 nm) was observed in {010}, {001}, and {110} growth sectors, whereas the red species (MR^{in}, 514 nm) was observed only in {001} and {110}. The deconvolution of the absorbance spectra in sectors containing both species was achieved by subtracting the spectrum of the pure yellow species found exclusively in {010} multiplied by a variable scaling factor (see Supporting Information). The difference spectra had the same λ_{max} for all polarizations and growth conditions.

The orientations of the four symmetry related electric dipole transition moments for MR^{in} and MR^{ex} were calculated from the dichroic ratios (Figure 8).[40] The angle with respect to the vibration directions in which it is measured is equal to the inverse tangent of the dichroic ratio to the −1/2 power. The orientation of the yellow species in {001}, {010}, and {110} is relatively invariant being 49, 46, and 44° from [010] in the (101) plane, respectively. The orientation of the red species in the (001) and (110) growth sectors was 40 and 62° from [010], respectively.

Mo Kα radiation from a sealed tube was indistinguishably diffracted from mixed PA/MR crystals and pure PA. It has been observed by us and others that sealed-tube X-ray scattering experiments are ill-suited to the analysis of dye inclusion crystals.[7,14,41]

Docking simulations of MR to the lowest energy surfaces of (001) and (110) were conducted using a molecular replacement approach. Comparable docking to (010) was not possible as neither H-bond donors nor acceptors are exposed; removal of multiple PAs would be necessary. Single PA molecules were

(36) For the spectral characteristics in a variety of polymer and glass matrices, see: Yariv, E.; Reisfeld, R.; Weiss, A. M. *SPIE* **1993**, *1972*, 46−54.

(37) (a) Etter, M. C. *Acc. Chem. Res*. **1990**, *23*, 120−126. (b) Etter, M. C.; MacDonald, J. C.; Bernstein, J. *Acta Crystallogr*. **1990**, *B46*, 256−262. (c) Bertnstein, J.; Davis, R. E.; Shimoni, L.; Chang, N.-L. *Angew. Chem., Int. Ed. Engl*. **1995**, *34*, 1555−1573.

(38) The benzoic acid and MR dimer were constructed in Gaussian 03 using the hybrid B3LYP functional and the 6-311G** basis set. The continuum IEFPCM solvation model was used with the water solvent parameters. The united atom model was used to construct the cavity, except for the two carboxylate groups, where explicit H atoms were used.

(39) The MR°, $MR^{\pm}$, and MRH^+ structures were taken from the 0.5 PA·MR, 2,5-DHB·MR, and MR·HBr·H_2O structures, respectively. MR^- was taken from Pruchnik, F. P.; Banbula, M.; Ciunik, Z.; Chojnacki, H.; Latocha, M.; Skop, B.; Wilczok, T.; Opolski, A.; Wietrzyk, J.; Nasulewicz, A. *Eur. J. Inorg. Chem*. **2002**, *12*, 3214−3221.

(40) Measurement of the dichroic ratio ($A_\perp/A_\parallel$) along vibration directions in a plane enables the calculation of the orientation of the electric dipole transition moments within the plane. A three-dimensional orientation of the electric dipole transition moments within the crystal lattice can be calculated from dichroic ratios obtained in two orthogonal planes. The small size of {021} prevented accurate absorbance measurements in this growth sector.

(41) (a) Foote, F. G.; Blake, F. C.; France, W. G. *J. Phys. Chem*. **1930**, *34*, 2236−2240. (b) Paine, P. A.; France, W. G. *J. Phys. Chem*. **1935**, *39*, 425−429.

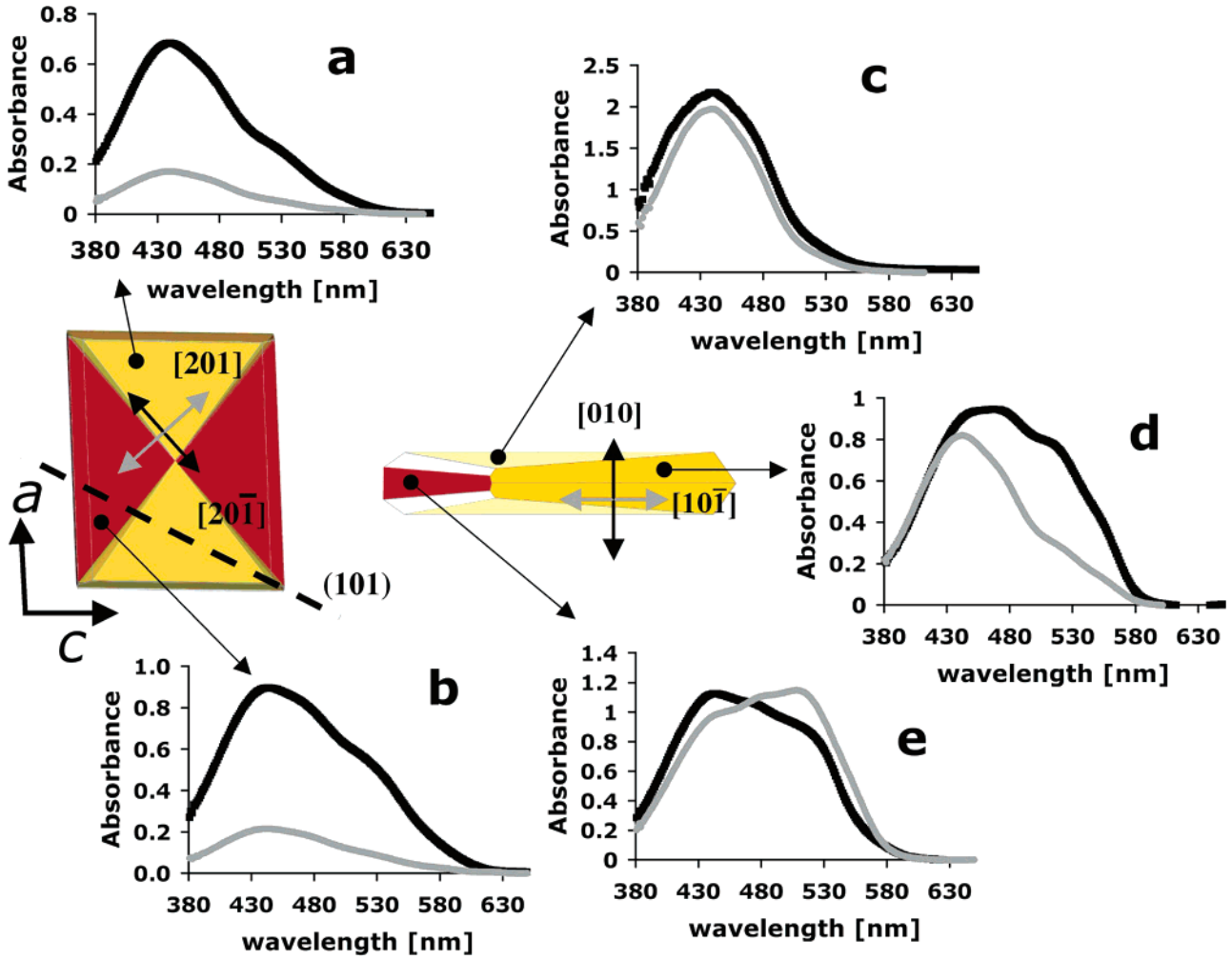

Figure 8. Polarized absorbance spectra of the various PA growth sectors dyed by MR. Vibration directions indicated are approximate. Input polarization direction: (a, b) [20$\bar{1}$] (black), [201] (gray); (c, d, e) [10$\bar{1}$] (black), [010] (gray).

removed from the 2-D periodic surfaces of the relaxed cell and replaced with MR, allowing for hydrogen bonding between COOH groups. Cerius2 was used to perform a constrained geometry optimization using the CVFF force field (Figure 9).[21,42] The PA atomic positions were fixed, and the energy of MR was minimized as a function of position with its geometry fixed. The (001) surface has a single PA molecule presentation. The (110) surface displays two PA molecules related by symmetry in the bulk but dissymmetric on the surface. These two sites are distinguished as I and II (Figure 9). The long axis of MR is inclined 40° with respect to [010], parallel to PA hydrogen bonds, when docked to (001) and position I on (110). When docked to position II on (110), MR is nearly parallel to [100].

Computational modeling of MR^{in} *within* the PA lattice was carried out to determine the lowest energy orientations for MR (Figure 10). The volume of two PA molecules, calculated from the crystal structure, is 349 Å^3. Likewise, the volume of one MR is 329 Å^3. Thus, we must remove at least two PA molecules from the lattice to accommodate one MR molecule. Assuming that MR is oriented approximately along [10$\bar{1}$] when viewed down [010], consistent with the LD, three distinct substitutions of one MR for two PA molecules in the CVFF minimized lattice were considered: the long axis of MR parallel to [001], parallel to [010], and parallel to a hydrogen-bound PA dimer. MR^{ex} parallel to a hydrogen-bound PA dimer, the only orientation possible to maintain proper hydrogen bonding geometry, was also analyzed. The MR geometry from the crystal structure was used to model MR^{in}. The MR geometry from the calculated $R_2^2(8)$ benzoic acid complex was used to model MR^{ex}.

Initially, energies were minimized with MR restrained as a rigid body within a fixed PA lattice. The restraints on the PA lattice were then removed, and the energy was again minimized. The replacement energies (REs) were calculated as

$$\mathrm{RE} = E_{mc} + n(E_{PA}) - (E_{pc}) + n(E_{MR})$$

where E_{mc} is the total minimized energy of the mixed crystal, $n(E_{PA})$ is the energy of n isolated phthalic acid molecules removed to accommodate the host, E_{pc} is the energy of the pure PA crystal, and $n(E_{MR})$ is the energy of n isolated MR molecules ultimately accommodated in the mixed crystal. Energies for various models are tabulated in Table 3.

Heating. Gaubert refined the concept of syncrystallization while heating heavily dyed PA/MR mixed crystals. We repeated his experiment in crystals with a PA/MR mol ratio of 5×10^{-5}. At 150 °C, the LD at 514 nm decreases and transmittance increases throughout the crystal.[43] We imaged the LD at 547 nm using the rotating polarizer technique (Figure 11).[43] After

(42) *Cerius2*, version 4.0; Molecular Simulations Inc.: San Diego, CA, 1999.

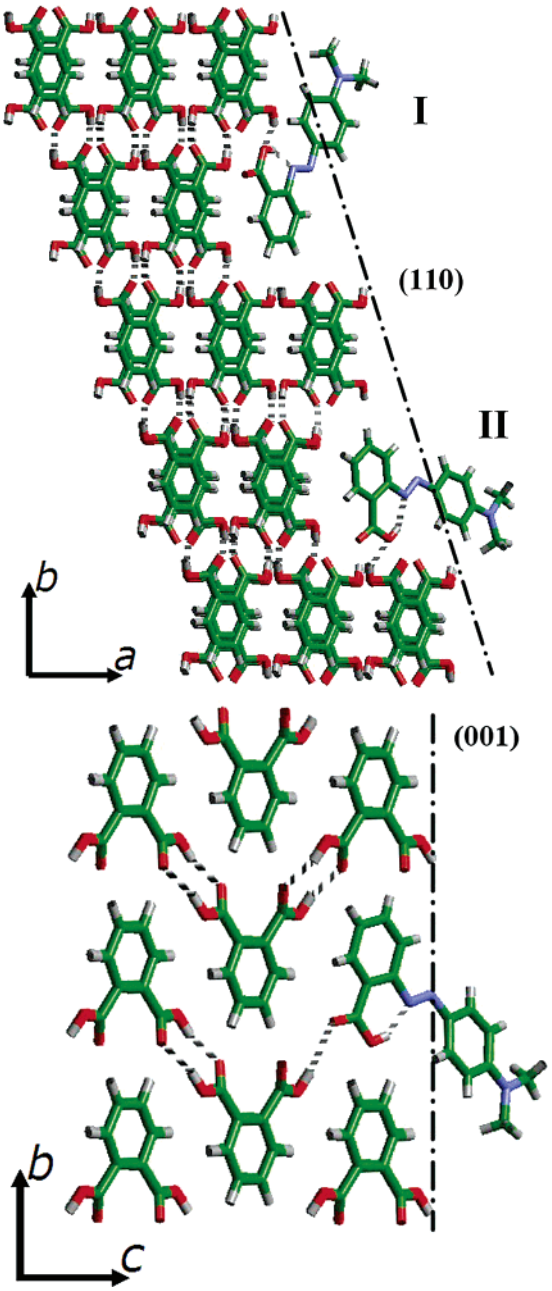

Figure 9. Simulations of MR^{in} docking to two distinct sites (I and II) on (110) above and one site on (001). Black dot-dashed lines denote lowest energy stable surfaces for the indicated facets.

heating for 10−15 min, dark spots called *bâtonnets* by Gaubert began to accumulate in the crystal (Figure 12). They grew lozenge-like with time along the cleavage planes. They advanced in the (010) planes perpendicular to the direction of elongation. Once the choice between symmetry related perpendicular directions in the centrosymmetric crystals was established, the bâtonnets never change direction. As they grew while traversing the crystal, they left behind red-dye-depleted wakes (Figure 12). The birefringence of the depleted areas was unperturbed, suggesting the bulk PA lattice reassembled in the wakes of the bâtonnets. The wakes remained orange and linearly dichroic, indicating that the diffusing species was MR^{in}. Analysis of the bâtonnets by micro-Raman spectroscopy indicated that they were rich in methyl red, but we could not unequivocally distinguish them as MR or as 0.5 PA·MR due to signal from the sea of host PA.

Discussion

Color. Our first task, when confronted with Gaubert's crystals, was to explain etiology of the different colors. The preponderance of evidence developed from mixed and cocrystals led to the conclusion that the difference between the yellow and red colors depended merely on whether the COOH proton was intramolecularly (MR^{in}) or intermolecularly (MR^{ex}) hydrogen bound. According to our ZINDO calculations, MR^{ex} is most like the basic MR^- species. MR^{in} is zwitterion-like, $MR^{\pm}$. Our experiments cannot determine whether the O···H···N proton is closer to O or N within PA. In any case, whether the intramolecular H-bonding does or does not represent a genuine tautomerism, electrons are drawn from $-N(CH_3)_2$, giving the MR considerable quinoidal character and a red color.

A lone 2001 paper, standing apart from the early 20th century studies of PA/MR, describes the dyeing of another aromatic acid, 2,5-dihydroxybenzoic acid (DHB), with MR.[44] DHB, unlike some of its constitutional isomers, is an effective MALDI (matrix-assisted laser desorption ionization mass spectrometry) matrix, but why it is effective remains a subject of active research. In an effort to determine whether ions observed by MALDI were preformed in the host matrices, Krüger et al. used acid−base indicators, such as MR, as analytes.[44] They reasoned that the color of the mixed crystals formed between dye and host could be taken as a clear indication of the protonation state of the dye in the solid state. DHB microcrystallites were red (judged only by eye, not with a spectrophotometer) when grown in the presence of MR, leaving the authors to conclude that the $M + H^+$ ion observed in the gas phase was preformed in the mixed crystals. From our work with MR and PA, we can conclude that the state of a solvatochromic acid−base indicator in a crystal is not simply judged by color. We must modulate this criticism by emphasizing that we had earlier made the identical rush to judgment.[7,45]

Face Selectivity and Polarization. The dominant intermolecular interaction in the 0.5 PA·MR cocrystal structure is H-bonding between PA and MR COOH groups (see Figure 13). We might then reasonably assume that the H-bond donating ability of different surfaces might explain their selectivity for MR. The lowest energy surfaces of the expressed faces (110) and (001) are shown in Figure 9. Indeed, both surfaces have exposed COOH groups and incorporate MR^{in}.

The long axis of MR^{in} projected in (101) was inclined ~40° from *b* when docked to the one unique site on (001) (Figure 8), in agreement with the dichroic ratio (see previous section). On the other hand, two unique positions are available for docking to (110): MR^{in} inclined approximately 40° from *b* and approximately parallel to *a*. Dichroic ratios for the (110) sector indicate that MR^{in} is oriented in (101) projection on average

(43) Glazer, A. M.; Lewis, J. G.; Kaminsky, W. *Proc. R. Soc. London A* **1996**, *452*, 2751−2765.

(44) Krüger, R.; Pfenninger, A.; Fournier, I.; Glückman, M.; Karas, M. *Anal. Chem.* **2001**, *73*, 5812−5821.

(45) Kurimoto, M.; Bastin, L. D.; Fredrickson, D.; Gustafson, P. N.; Jang, S.-H.; Kaminsky, W.; Lovell, S.; Mitchell, C. A.; Chmielewski, J.; Kahr, B. In *Morphology and dynamics of crystal surfaces in complex molecular systems*; De Yoreo, J. J., Casey, W. H., Malkin, A. J., Vlieg, E., Ward, M. D., Eds.; Materials Research Society: Pittsburgh, 2001; Vol. 620, pp M981−M9810.

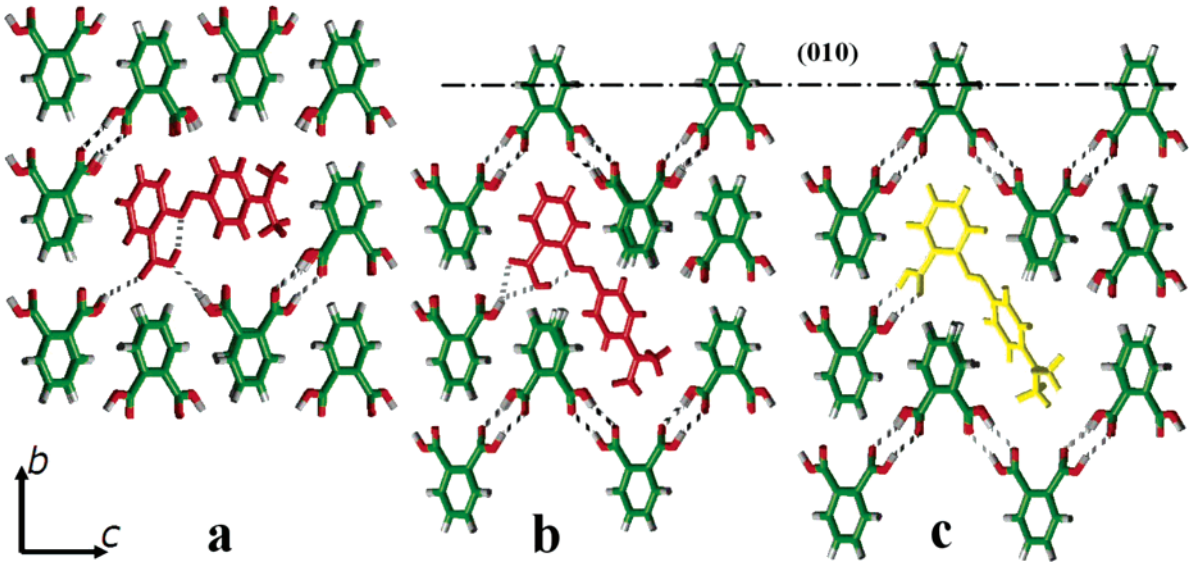

Figure 10. Models of MR^{in} (red) and MR^{ex} (yellow) within the PA lattice. (110) contains the MR species in **a**, **b**, and **c**; (001) contains only **b** and **c**; (010) contains only **c**. Lowest energy (010) surface denoted by dashed black line.

Table 3. Computed Replacement Energies (RE) for Mixed Crystal Models

model	guest orientation	RE (kcal/mol)
Figure 10a	MR^{in} parallel to [001]	76.9
not shown	MR^{in} parallel to [010]	82.4
Figure 10b	MR^{in} parallel to PA H-bonds	74.2
Figure 10c	MR^{ex} as $R_2^2(8)$ dimer	72.3

62° from *b*. Thus, a combination of both orientations in a ratio of 3:5, respectively, would give rise to this intermediate average orientation.

MR^{in} model I adsorbed to (110) (Figure 9) and MR adsorbed to (001) give rise to the orientation inside the crystal pictured in Figure 10b. MR^{in} model II adsorbed to (110) (Figure 9) gives rise to the orientation inside the crystal pictured in Figure 10a. The difference in replacement energies between models 10a and 10b is less than 3 kcal/mol (Table 3). The third calculated orientation consistent with the replacement of one MR for two PAs, that with MR^{in} parallel to *b*, is nearly 6 kcal/mol higher in energy than MR^{in} parallel to *a*. No stable surfaces can dock MR^{in} parallel to *b* via H-bonding. This geometry is not found within the PA crystals examined. It is not illustrated and is not considered further.

MR^{ex} was found in every sector. Unlike MR^{in}, the $R_2^2(8)$ hydrogen bonding constraint permits only one orientation for this species within the PA lattice. The RE for the MR^{ex} inclusion was determined to be 2 kcal/mol less than the lowest energy MR^{in} inclusion. Furthermore, the computed orientation of MR^{ex} is 4° closer to [100] than MR^{in}, which agrees with the dichroic ratios.

Phase Separation. On heating PA/MR, the principal observation is the loss of dichroism for the low energy band when light is incident on (010). Loss of dichroism is consistent with the rotation of a subpopulation of MR^{in} molecules by approximately 90° around *b*. Such a reorientation would position the molecules with respect to PA as is found in 0.5 PA·MR. Could microscopic 0.5 PA·MR domains form within PA/MR mixed crystals? Might we consider this process a syncrystallization but one that could not have been forecast in earlier generations because the structure of 0.5 PA·MR had not been established?

The similarities between the crystals of PA and MR, with cocrystals 0.5 PA·MR, are striking. For example, the disposition of rows of PA molecules in cocrystals matches very well with every fourth PA row in the pure crystal (Figure 13). A more quantitative comparison is achieved by describing the 2-D periodicity of the sheets of the "pure" substances in the cocrystal, as well as matching planes in the pure crystals, by two vectors and the angle between them. The spatial distribution of the individual components in a plane in the cocrystal agrees quite well with planes found in the respective pure lattices (Table 4). By choosing a hydrogen-bonded tetrad consisting of a MR dimer and two PA molecules from the cocrystal, and superimposing the PA molecules of this tetrad onto the PA positions of the cocrystal, we find that the MR dimers are inclined by 82° with respect to the aromatic planes of PA layers in the pure acid. This model for the mixed crystals would imply that the polarization of maximum absorbance should be along [201]. This model is inconsistent with the polarization of MR^{in} in the mixed crystals that absorbs light maximally when the polarization is along [20 $\bar{1}$]. Inferences of guest orientations within a host, established on the basis of the analysis of cocrystal structures—even when remarkable correspondences between the pure and cocrystal structures exist—should be drawn cautiously. The traditional importance of lattice matching in the overgrowth of one substance on another has been de-emphasized by Ward and co-workers in their studies of edge-directed epitaxy.[46]

MR^{in} migrates within PA crystals following prolonged heating. It ultimately aggregates to form bâtonnets which then also migrate through the crystal. By contrast, the yellow species remains fixed within the lattice at elevated temperatures. This behavior is consistent with the model in which MR^{ex} is held tightly in place through the comparatively strong $R_2^2(8)$ hydrogen bonds. The hydrogen bonds between MR^{in} and the lattice lack the specificity and complementarity of MR^{ex}, allowing for

(46) (a) Bonafede, S. J.; Ward, M. D. *J. Am. Chem. Soc.* **1995**, *117*, 7853−7861. (b) Carter, P. W.; Ward, M. D. *J. Am. Chem. Soc.* **1993**, *115*, 11521−11535.

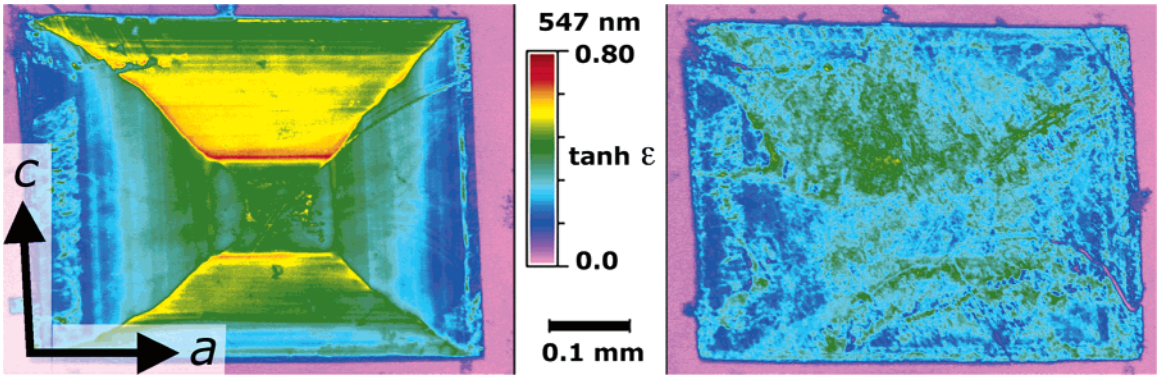

Figure 11. Linear dichroism images of PA/MR crystal grown on a glass slide (left) before heating and (right) after heating at 150 °C for 2 h. Tanh (ϵ) = $(T' - T'')/(T' + T'')$ (see Experimental Section).

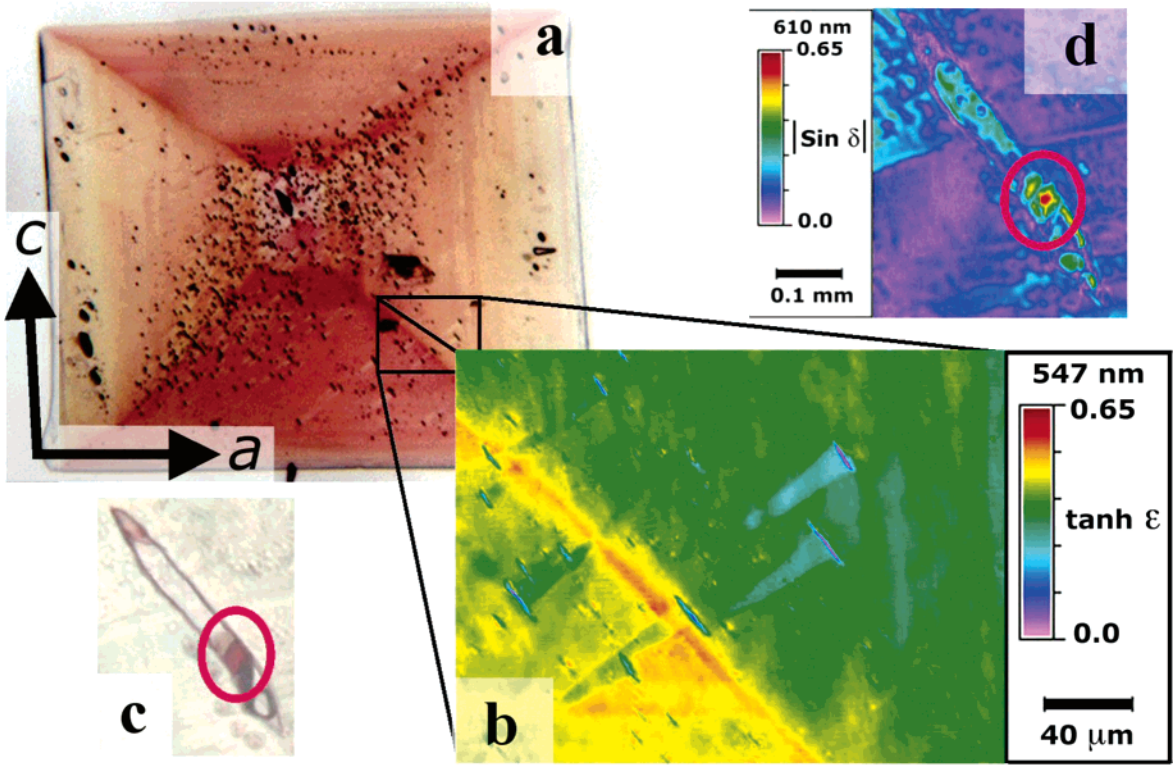

Figure 12. (a) PA/MR mixed crystal heated at 150 °C for 15 min and cooled to room temperature showing appearance of dark bâtonnets. (b) Linear dichroism image showing migration of bâtonnets. (c) Photograph of a bâtonnet after cooling, and (d) the corresponding linear birefringence image showing the high birefringence, circled in red, of the syncrystal. $\delta = 2\ \pi\Delta nL/\lambda$ (see Experimental Section).

rearrangement and migration when heated. The unidirectional migration is most probably a consequence of initial fluctuations leading to a small MR-rich aggregate. As PA recrystallizes in spaces vacated by MR^{in}, it presumably lowers the free energy of the crystal and drives the aggregate in the direction opposing the recrystallization. To the extent that MR-rich crystals can be oriented within dyed PA, we can fairly state that we have witnessed a syncrystallization.

Conclusions: What is Syncrystallization?

Adjacent growth sectors of phthalic acid crystals grown from solutions containing MR are alternately yellow and red. The color difference is not a consequence of acid−base chemistry as earlier conjectured.[7] Rather, it is a consequence of the H-bond acceptor (intramolecular or intermolecular) to which neutral MR directs is COOH proton. The intermolecularly H-bound yellow species (MR^{ex}) is less selectively included in the crystal, while the red dipolar species (MR^{in}) is associated with hydrogen bonding surfaces. Sorting out the chromo-chemistry in PA/MR necessitated a detailed investigation into the structure of MR in various environments. We have thus compared MR crystal structures containing the neutral, zwitterionic, and protonated forms. The intermolecular interactions between MR and PA that were observed in cocrystals failed to predict the polarization of the MR in the mixed crystals. The absorption anisotropy could only be reckoned by considering the docking of MR to the most stable computed surfaces and the REs associated with variously oriented MRs within the PA lattice.

PA precipitation from MR-containing solutions, of whatever relative concentration, does not yield PA crystals containing

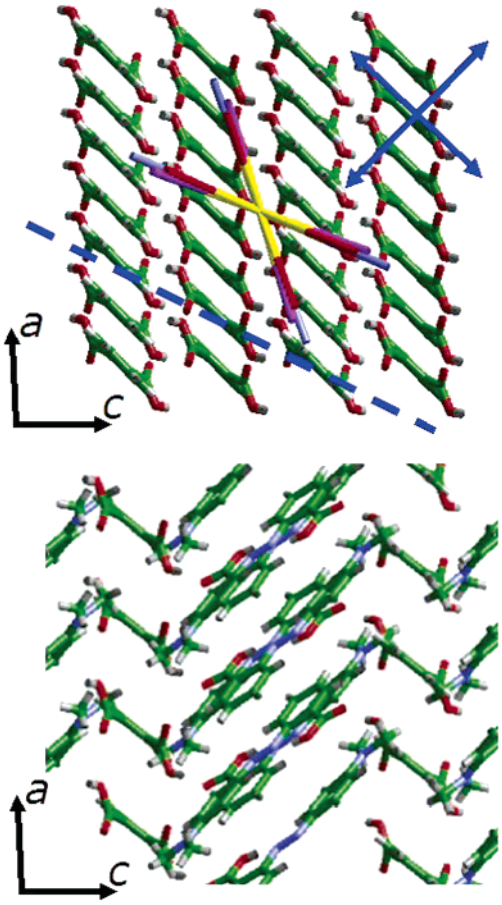

Figure 13. (Top) Experimental MR orientations superimposed upon the PA lattice for the red species in {001} (red tips), red species in {110} (blue tips), and averaged MR (purple tips). Dashed blue line is the (101) cleavage plane. (Bottom) Cocrystal structure of 0.5 PA·MR shows remarkable agreement with respect to PA sheets in both structures. The MR positions are inconsistent with polarized absorbance data for the mixed crystals.

Table 4. Similarities between 0.5 PA·MR Structure and Respective Pure Crystal Structures

	MR	MR plane of cocrystal	% difference
side 1	[100] = 8.235 (Å)	[110] = 8.422 (Å)	−2.27
side 2	[110] = 9.160 (Å)	[100] = 9.083 (Å)	0.84
angle	58.3°	57.4°	1.54
	PA	**PA plane of cocrystal**	**% difference**
side 1	[010] = 14.318 (Å)	[010] = 14.185 (Å)	0.93
side 2	[001] = 9.630 (Å)	[100] = 9.083 (Å)	5.68
angle	90°	90°	0

oriented microcrystals of MR. The interpretation of *syncrystallization* in the PA/MR system as an oriented overgrowth is baseless. Heating of the mixed crystals causes a MR reorientation, followed by a phase separation and recrystallization of a MR-rich phase. Establishing whether these dynamic processes are consistent with the notion of syncrystallization is facilitated by placing the Gaubert/Neuhaus papers within the context of accepted terminology for the phenomena of regular mutual orientation of crystals of disparate substances.[47]

Epitaxy, the concept championed by Neuhaus, is used to describe the oriented growth of one substance on the crystal surface of another substance. Minerologists use *syntaxy*[48] to describe the simultaneous growth of mutually oriented crystals of two or more phases. Syntaxy is an accepted contemporary substitute for syncrystallization. *Endotaxy*[49] is used to designate oriented segregation taking place in the bulk of a crystal. Endotaxy embodies the process of exsolution, the disintegration of solid solutions where the inclusions of a new phase are regularly oriented within the matrix. The terms *anomalous mixed crystals*, *partial-isomorphic mixed systems* (proposed by Spangenberg and Neuhaus[50]), and *adsorption mixed crystals*[51] have been proposed to account for oriented overgrowths/intergrowths/inclusions, but these terms have failed to gain wide currency.

Loss of MR dichroism on heating is consistent with MR reorientation so as to form supramolecular ensembles that resemble the 0.5 PA·MR cocrystals. Strictly speaking, this process could well be considered endotactic, although the microcrystals formed may not be bigger than a few MR molecules.

The recrystallization of a MR-rich phase within PA/MR mixed crystals may also be considered endotactic. We reemphasize that this is not the epitaxial cocrystallization assumed by Neuhaus.[18]

Other potential examples of syncrystallization/syntaxy of dyes with transparent host crystals from Gaubert's repertoire include methylene blue with lead nitrate[52] or urea oxalate.[53] The understanding of these phenomena and others[54] could similarly benefit from contemporary reinvestigations. This is not to say that there are not bona fide examples of two discrete substances crystallizing together in which one crystal serves as host to oriented crystallites of another. A classic example of such a pathological system is that of ammonium chloride and urea.[55]

Experimental Section

Sample Preparation. PA and MR were purchased from Aldrich and used without further purification. The growth solutions for crystals grown in a dish were prepared by dissolving proper amounts of the solids in neat ethanol followed by dilution with deionized water (Barnsted NANOpure, 18.2 MΩ/cm). Dye concentrations were based upon the molar concentration of initial growth solution volume. Solutions were evaporated in a dark cabinet at ambient temperature (23 °C). To grow microscopic crystals on glass slides, a saturated aqueous solution of PA was heated to approximately 50 °C. One milliliter of the hot solution was placed on a microscope slide with appropriate volumes of a 1.0 mg/mL ethanol solution. Crystals grew in approximately 20 min. The slide was then rinsed with hexane.

Crystals of MR suitable for X-ray diffraction were obtained by cooling a saturated hot toluene solution to room temperature. Crystals of 0.5 PA·MR were obtained by slow evaporation of an acetone solution containing 50 mg of MR and 31 mg of PA. Crystals of MR·HBr·H_2O were obtained by slow evaporation of 60 mL of methanol containing 100 mg of MR and 0.968 mL of 48% HBr in H_2O. Crystals of 2,5-DHB·MR were obtained by slow evaporation of a saturated ethanol solution containing 0.10 g of MR and 1.0 g of 2,5-DHB.

(47) (a) Bonev, I. *Acta Crystallogr.* **1972**, *A28*, 508−512. (b) Bailey, S. W.; Frank-Kamenetskii, V. A.; Godsztaub, S.; Kato, A.; Pabst, A.; Schulz, H.; Taylor, H. F. W.; Fleischer, M.; Wilson, A. J. C. *Acta Crystallogr.* **1977**, *A33*, 681−684.

(48) Ungemach, H. *Bull. Soc. Fr. Miner. Crist.* **1935**, *58*, 97−221; *Z. Kristallogr.* **1935**, *91*, 1−22.

(49) Palatnik, L. S.; Papirov, I. I. *Oriented Crystallization*; Metallurgia, Moscow, 1964; Cistijakov, Ju. D.; Schneider, H. G.; Weinhold, C. *Epitaxie-Endotaxie*; Leipzig: Deutsches Verlag für Grundstoffindustrie, 1969.

(50) Spangenberg, K.; Neuhaus, A. *Chem. Erde* **1930**, *5*, 437−528.

(51) Kleber, W. *Z. Phys. Chem.* **1959**, *212*, 222−234.

(52) Gaubert, P. *Comptes Rendus Acad. Sci. Paris* **1925**, *180*, 378−380.

(53) Gaubert, P. *Comptes Rendus Acad. Sci. Paris* **1918**, *167*, 491−494.

(54) Seifert, H. *Fortschr. Min. Kristallogr. Petro.* **1935**, *19*, 103−182; **1936**, *20*, 324−456; **1937**, *22*, 187−488.

(55) Punin, Yu. O.; Ivanova, T. I.; Kotelnikova, E. N.; Franke V. D. *Zapiski Vserossiiskogo Mineralogicheskogo Obschestva* **1993**, *122*, 26−36.

Physical Measurements. Solution spectra were obtained with the cuvette sampling bench of the SI Photonics model 440 UV/Vis spectrophotometer. Crystal absorption spectra were obtained by coupling the spectrometer to an Olympus BX50 transmission microscope via a 200 μm fiber-optic. The extinction directions of the crystals were used to orient the sample relative to the input polarization. Instec HS400 heating stage with a platinum resistance temperature detector was used to drive the formation of the bâtonnets.

To quantify linear anisotropies, we have employed the rotating polarizer technique as embodied in the Metripol microscope.[43] The optical train consists of a filter as monochromator, a mechanically rotating polarizer, a sample inducing the phase shift δ, a quarter wave retarder, and a polarizer aligned at 45° toward the quarter wave plate's eigenray directions:

$$\mathbf{A}' = \mathbf{M}_{45-\mathrm{pol}}\mathbf{M}_{\lambda/4}\mathbf{M}_{\mathrm{sample}}\mathbf{R}_{\theta}\mathbf{J}_{x}$$

where $\mathbf{J}_x$ is the Jones matrix[56] for linearly polarized light operated on by a rotation matrix ($\mathbf{R}_\theta$), and Jones matrices representing the sample that is linearly birefringent ($\mathbf{M}_{\mathrm{sample}}$), a quarter wave plate ($\mathbf{M}_{\lambda/4}$), and a linear polarizer ($\mathbf{M}_{45-\mathrm{pol}}$). The position of the sample with respect to the rotating polarizer is defined by the angle θ, $\theta = \alpha - \phi$, where α is the rotation angle of the polarizer and ϕ the angle between the slow vibration direction of the sample and the polarizer when $\alpha = 0$. From the amplitudes, the normalized intensity I/I_0 is found directly as

$$\frac{I}{I_0} = A'^{*} \cdot A' = 2\cdot\frac{1}{4}[(\cos\theta e^{ix} - \sin\theta e^{-ix})(\cos\theta e^{-ix} - \sin\theta e^{ix})] = \frac{1}{2}[1 + \sin 2(\alpha - \phi)\sin\delta]$$

In the Metripol method, intensity measurements at discrete steps (α_i) generate expressions that are easily converted to linear polynomials. Data collected over full periods yield Fourier coefficients from which the variable parameters are extracted analytically.

Simple modifications of the optical train permit the measurement of LD.[57] The anisotropic absorption may be determined by removing the quarter wave plate and analyzer. The Jones vector for a LD measurement using MetriPol is

$$\mathbf{A}' = \mathbf{M}_{\mathrm{LD,LB}}\mathbf{R}_{\theta}\mathbf{A}_{x}$$

$$\mathbf{A}' = t\cdot\begin{bmatrix} t_x e^{i(\delta/2)} & 0 \\ 0 & t_y e^{-i(\delta/2)} \end{bmatrix}\cdot\begin{bmatrix} \cos\theta & \sin\theta \\ -\sin\theta & \cos\theta \end{bmatrix}\cdot\begin{bmatrix} 1 \\ 0 \end{bmatrix} = t\cdot\begin{bmatrix} t_x e^{i(\delta/2)}\cos\theta \\ -t_y e^{-i(\delta/2)}\sin\theta \end{bmatrix}$$

where t is the average transmission coefficient, $t_{x/y}$ are the transmission coefficients in the x, y directions, and θ is the initial angle between the polarizer and the slow vibration direction of the sample. After some manipulation,[56] we can relate $\tanh\epsilon$ (ϵ is the difference between optical densities in orthogonal directions) to the orthogonal transmission terms T''' giving

$$\tanh\epsilon = \frac{\sinh\epsilon}{\cosh\epsilon} = \frac{(e^{+\epsilon} - e^{-\epsilon})/2}{(e^{+\epsilon} + e^{-\epsilon})/2} = \frac{T' - T''}{T' + T''}$$

X-ray Crystallography. Crystals were indexed with a Stoe 2-circle Model J optical goniometer and a Nonius KappaCCD diffractometer. Data were collected with the KappaCCD using Mo Kα radiation (λ = 0.71073 Å). Integration of intensities and cell refinement was carried out using HKL2000[58] and HKL SCALEPACK, respectively. Solution by direct methods (SIR97)[59] produced a complete heavy atom phasing model consistent with the proposed structure. Structures were refined using SHELXL-97.[60] Non-hydrogen atoms were refined anisotropically by full-matrix least squares. All hydrogen atoms were refined with a riding model.

Acknowledgment. B.K. thanks the National Science Foundation and the donors to the Petroleum Research Fund of the American Chemical Society for support of this research. A.R. acknowledges the Merit Allocation Scheme of the National Facility of the Australian Partnership for Advanced Computing, without which the first principle calculations would not have been possible. We are grateful for Dr. Brian Marquardt's assistance and the early contributions of Dr. Christine Mitchell.

Supporting Information Available: Example of spectral deconvolution. Spectra of heating experiments. Crushed crystal spectra. X-ray crystallographic data in CIF format for all crystal structures reported. Coordinates for all mixed crystal models. Complete ref 31. This material is available free of charge via the Internet at http://pubs.acs.org.

JA0601181

(56) Kaminksy, W.; Claborn, K.; Kahr, B. *Chem. Soc. Rev.* **2004**, *33*, 514−525.
(57) Kaminksy, W.; Jin, L.-W.; Powell, S.; Maezawa, I.; Claborn, K.; Branham, C.; Kahr, B. *Micron*, doi:10.1016/j.micron.2005.10.014.
(58) Owtinoski, Z.; Minor, W. *Methods Enzymol.* **1996**, *276*, 307−326.
(59) Altomare, A.; Cascarano, G.; Giacovazzo, C.; Guargliari, A.; Burla, M. C.; Polidori, G.; Camalli, M. *J. Appl. Crystallogr.* **1997**, *27*, 435−442.
(60) Sheldrick, G. M. *SHELXL-97*; University of Göttingen: Germany, 1997.